Journal of Sound and Vibration (1998) **214**(3), 580–587
Article No. sv981568

DIAMETRAL PLANE-WAVE ANALYSIS FOR SHORT CIRCULAR CHAMBERS WITH END OFFSET INLET/OUTLET AND SIDE EXTENDED INLET/OUTLET

A. Selamet and Z. L. Ji

Department of Mechanical Engineering and The Center for Automotive Research, The Ohio State University, Columbus, OH 43210-1107, *U.S.A.*

(*Received* 19 *February* 1998)

1. INTRODUCTION

In some applications of expansion chambers where the frequency range of interest is low, the planar wave analysis becomes useful for an estimate of the acoustic performance. For long symmetric expansion chambers, Davis *et al*. [1] introduced a one-dimensional (1-D) analytical approach by assuming linear plane wave propagation in the axial direction. For the circular expansion chambers with 180° offset inlet/outlet, recent investigations [2, 3] illustrated, below the cut-off frequency of the first diametral (1, 0) mode, a nearly one-dimensional wave propagation along the diametral direction for configurations with a length to diameter ratio $l/d < 0{\cdot}853$, and axial wave propagation for $l/d > 0{\cdot}853$. This particular ratio, $l/d = 0{\cdot}853$, is used hereafter in this paper to distinguish the "short" and "long" chambers with 180° offset inlet/outlet.

The objective of the present study is to provide a diametral plane wave analysis for *short* chambers in the absence of mean flow (see, for example, reference [4] for this effect). By assuming a 1-D wave propagation in the diametral direction and using the segmentation approach (see reference [5] for the convergence of this approach), the present study develops the four-pole parameters of the chambers with *end offset inlet/outlet* and *side extended inlet/outlet*, which are then used to determine the transmission loss. The boundary element method (BEM) is also employed to assess the accuracy of the 1-D diametral predictions.

2. FORMULATION

Consider the expansion chambers of Figure 1 with (a) end offset inlet/outlet and (b) side extended inlet/outlet. These chambers are divided into three sections designated by a, b and c. Note that a simple side inlet/outlet chamber is the limit of configuration (b) with no extensions. By assuming plane wave propagation in the diametral direction and using

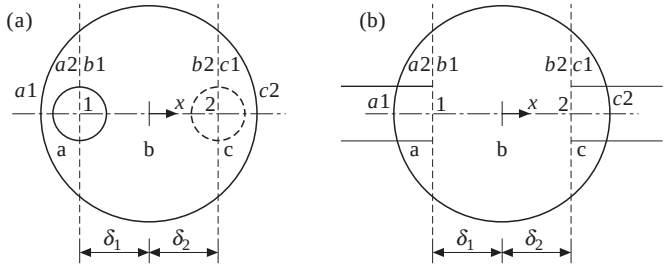

Figure 1. (a) End offset inlet/outlet chamber and (b) side extended inlet/outlet chamber.

0022–460X/98/280580 + 08 $30.00/0

the continuity conditions of the acoustic pressure and volume velocity at interfaces lead to

$$\begin{bmatrix} P_1 \\ \rho c U_1 \end{bmatrix} = \begin{bmatrix} 1 & 0 \\ S_{a2}/(S_1 Z_a) & S_{b1}/S_1 \end{bmatrix} \begin{bmatrix} P_{b1} \\ \rho c U_{b1} \end{bmatrix}, \qquad \begin{bmatrix} P_{b2} \\ \rho c U_{b2} \end{bmatrix} = \begin{bmatrix} 1 & 0 \\ S_{c1}/(S_{b2} Z_c) & S_2/S_{b2} \end{bmatrix} \begin{bmatrix} P_2 \\ \rho c U_2 \end{bmatrix}, \tag{1, 2}$$

where P, U, ρ, c and S are the acoustic pressure, particle velocity, medium density, speed of sound, and the cross-sectional area, respectively; the subscripts 1 and 2, $b1$ and $b2$, and $a2$ and $c1$ denote the inlet and outlet of the chamber, the two ends of the central cavity b, and the boundaries of the two end cavities a and c neighboring cavity b, respectively;

$$Z_a = -P_{a2}/(\rho c U_{a2}), \qquad Z_c = P_{c1}/(\rho c U_{c1}), \tag{3, 4}$$

are the characteristic impedances of the two end cavities a and c. In terms of the transfer matrix approach, the following expressions may be written for the two end cavities:

$$\begin{bmatrix} P_{a1} \\ \rho c U_{a1} \end{bmatrix} = \begin{bmatrix} T^{\,a}_{11} & T^{\,a}_{12} \\ T^{\,a}_{21} & T^{\,a}_{22} \end{bmatrix} \begin{bmatrix} P_{a2} \\ \rho c U_{a2} \end{bmatrix}, \qquad \begin{bmatrix} P_{c1} \\ \rho c U_{c1} \end{bmatrix} = \begin{bmatrix} T^{\,c}_{11} & T^{\,c}_{12} \\ T^{\,c}_{21} & T^{\,c}_{22} \end{bmatrix} \begin{bmatrix} P_{c2} \\ \rho c U_{c2} \end{bmatrix}. \tag{5, 6}$$

By using the rigid wall boundary condition, set $U_{a1} = 0$ in equation (5) and $U_{c2} = 0$ in equation (6) to get respectively

$$Z_a = T^{\,a}_{22}/T^{\,a}_{21}, \qquad Z_c = T^{\,c}_{11}/T^{\,c}_{21}. \tag{7, 8}$$

The acoustic pressures and particle velocities at two ends of the central cavity b are related by

$$\begin{bmatrix} P_{b1} \\ \rho c U_{b1} \end{bmatrix} = \begin{bmatrix} T^{\,b}_{11} & T^{\,b}_{12} \\ T^{\,b}_{21} & T^{\,b}_{22} \end{bmatrix} \begin{bmatrix} P_{b2} \\ \rho c U_{b2} \end{bmatrix}, \tag{9}$$

where $T^{\,b}_{ij}$'s are the four-pole parameters of the central cavity. Combining equations (1), (2) and (9) yields

$$\begin{bmatrix} P_1 \\ \rho c U_1 \end{bmatrix} = \begin{bmatrix} 1 & 0 \\ S_{a2}/(S_1 Z_a) & S_{b1}/S_1 \end{bmatrix} \begin{bmatrix} T^{\,b}_{11} & T^{\,b}_{12} \\ T^{\,b}_{21} & T^{\,b}_{22} \end{bmatrix} \begin{bmatrix} 1 & 0 \\ S_{c1}/(S_{b2} Z_c) & S_2/S_{b2} \end{bmatrix} \begin{bmatrix} P_2 \\ \rho c U_2 \end{bmatrix}$$

$$= \begin{bmatrix} T_{11} & T_{12} \\ T_{21} & T_{22} \end{bmatrix} \begin{bmatrix} P_2 \\ \rho c U_2 \end{bmatrix}, \tag{10}$$

which defines the four-pole parameters of the entire chamber, T_{ij}, in terms of Z_a and Z_c of equations (7) and (8) for the two end cavities, and $T^{\,b}_{ij}$ of the central cavity. The transmission loss of an anechoically terminated chamber is given by

$$TL = 20 \log_{10} \{\tfrac{1}{2} | T_{11} + T_{12} + T_{21} + T_{22} |\} + 10 \log_{10}(S_1/S_2). \tag{11}$$

The calculation of T_{ij} and therefore the transmission loss of equation (11) involve T^{a}_{ij}, $T^{\,c}_{ij}$, and $T^{\,b}_{ij}$ of equations (5), (6) and (9). To determine these three matrices, the two end cavities and the central cavity are modelled as a series of conical duct segments with a rectangular cross-section of depth l. The four-pole parameters for such segment are

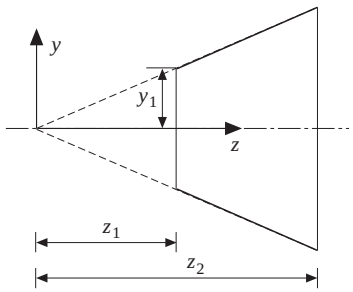

Figure 2. A conical duct with a rectangular cross-section of constant depth.

developed next. The sound propagation in a duct with varying cross-sectional area is given [6] by

$$\mathrm{d}^2P/\mathrm{d}z^2 + (1/S(z))(\mathrm{d}S(z)/\mathrm{d}z)\,\mathrm{d}P/\mathrm{d}z + k^2P = 0, \tag{12}$$

where $S(z)$ is the cross-sectional area at z. For the conical duct of Figure 2 with a rectangular cross-section, the cross-sectional area at z *is*

$$S(z) = 2yl = 2(y_1/z_1)zl, \tag{13}$$

which reduces equation (12) to

$$\mathrm{d}^2P/\mathrm{d}z^2 + (1/z)\,\mathrm{d}P/\mathrm{d}z + k^2P = 0. \tag{14}$$

The solution of equation (14) may be expressed as

$$P(z) = AJ_0(kz) + BY_0(kz) \tag{15}$$

which also yields, through the momentum equation, the particle velocity as

$$U(z) = -\mathrm{j}/(\rho c)[AJ_1(kz) + B\mathrm{Y}_1(kz)], \tag{16}$$

where J_m and Y_m are the mth order Bessel functions of the first and the second kind, respectively. The four-pole parameters of an arbitrary conical segment 'i' are then obtained as

$$T_{11}^{(i)} = P_1^{(i)}/P_2^{(i)}|_{U_2^{(i)}=0} = (\pi/2)kz_2[\mathrm{J}_1(kz_2)\mathrm{Y}_0(kz_1) - \mathrm{J}_0(kz_1)\mathrm{Y}_1(kz_2)], \tag{17a}$$

$$T_{12}^{(i)} = P_1^{(i)}/(\rho c U_2^{(i)})|_{P_2^{(i)}=0} = \mathrm{j}(\pi/2)kz_2[\mathrm{J}_0(kz_1)\mathrm{Y}_0(kz_2) - \mathrm{J}_0(kz_2)\mathrm{Y}_0(kz_1)], \tag{17b}$$

$$T_{21}^{(i)} = \rho c U_1^{(i)}/P_2^{(i)}|_{U_2^{(i)}=0} = -\mathrm{j}(\pi/2)kz_2[\mathrm{J}_1(kz_2)\mathrm{Y}_1(kz_1) - \mathrm{J}_1(kz_1)\mathrm{Y}_1(kz_2)], \tag{17c}$$

$$T_{22}^{(i)} = U_1^{(i)}/U_2^{(i)}|_{P_2^{(i)}=0} = (\pi/2)kz_2[\mathrm{J}_1(kz_1)\mathrm{Y}_0(kz_2) - \mathrm{J}_0(kz_2)\mathrm{Y}_1(kz_1)]. \tag{17d}$$

The transfer matrix of a structure consisting of, for example, n conical segments are determined by $[T] = \Pi_{i=1}^{n}[T^{(i)}]$, which are subsequently used in equations (5), (6) and (9).

3. RESULTS AND DISCUSSION

Consider an example for the expansion chamber with the end offset inlet/outlet: the configuration 1 of reference [3] ($l = 0{\cdot}0314$ m, $d = 0{\cdot}1532$ m, $d_1 = d_2 = 0{\cdot}0486$ m, $\delta_1 = \delta_2 = 0{\cdot}0510$ m) with a cut-off frequency of first diametral mode $f_{10} = 1324$ Hz. The transmission loss calculations for this chamber used a total of 32 conical segments. When the number of segments are doubled to 64, the results remain nearly the same throughout the frequency range of interest in the present study (at the highest frequency of $f = 1600$ Hz, the deviation in the transmission loss is 0·65%), suggesting that 32 conical

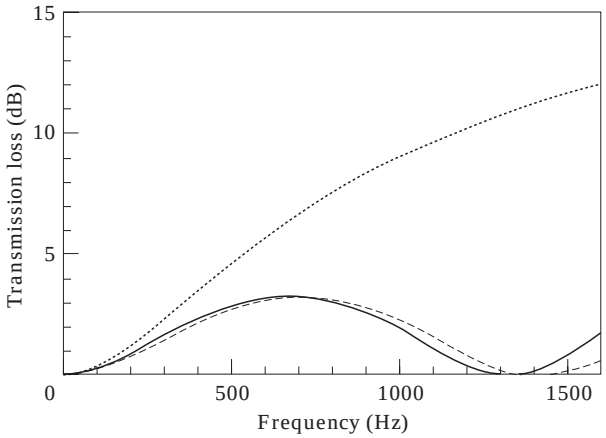

Figure 3. Transmission loss of a short chamber with end offset inlet/outlet ($d = 0{\cdot}1532$ m, $l = 0{\cdot}0314$ m, $d_1 = d_2 = 0{\cdot}0486$ m, $\delta_1 = \delta_2 = 0{\cdot}0510$ m): ——, 1-D diametral; ·····, 1-D axial; - - - -, BEM.

segments are adequate for accuracy within 1%. Figure 3 compares the transmission loss results from 1-D diametral model, 1-D axial model and the BEM. A reasonable agreement is observed between the 1-D diametral and the BEM predictions at low frequencies, while no similarity exists between this pair and the 1-D axial predictions. Moving the inlet and oulet towards the axis of the expansion chamber increases the difference between the 1-D diametral and the BEM solutions with increasing frequencies, as progressively shown in Figures 3–5 (Figure 3: $\delta_1 = \delta_2 = 0{\cdot}0510$ m; Figure 4: $\delta_1 = \delta_2 = 0{\cdot}0340$ m; Figure 5: $\delta_1 = \delta_2 = 0{\cdot}0170$ m). For the limiting case of concentric configuration with the inlet and outlet on the same axis of the expansion chamber, the radial wave propagation dominates in the chamber. Based on the 1-D radial wave propagation in the chamber and using the continuity conditions of the acoustic pressure and volume velocity, the transmission loss of a chamber can be obtained, for $a_1 = a_2$, as

$$TL = 20 \log_{10}|1 + l/(a_1 Z_{ch})|, \tag{18}$$

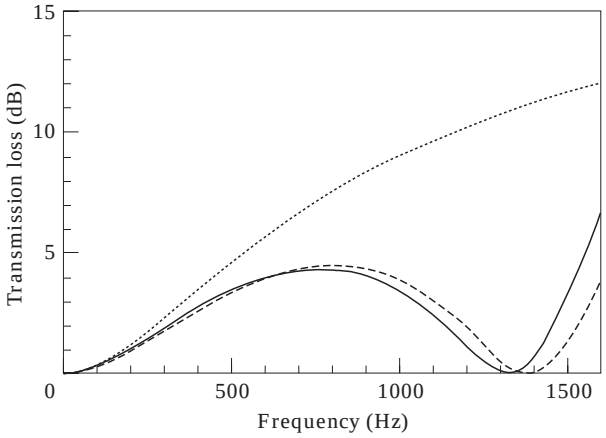

Figure 4. Transmission loss of a short chamber with end offset inlet/outlet ($d = 0{\cdot}1532$ m, $l = 0{\cdot}0314$ m, $d_1 = d_2 = 0{\cdot}0486$ m, $\delta_1 = \delta_2 = 0{\cdot}0340$ m): ——, 1-D diametral; ·····, 1-D axial; - - - -, BEM.

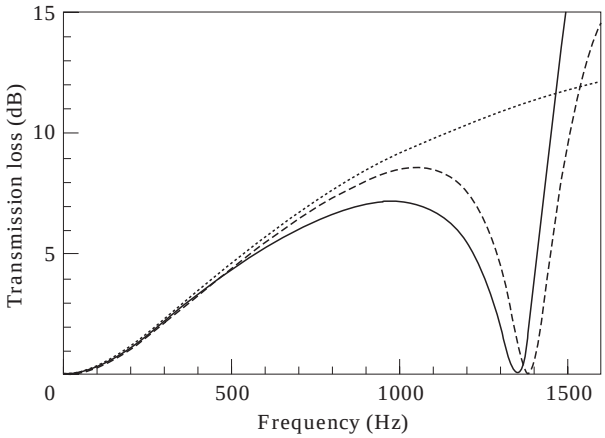

Figure 5. Transmission loss of a short chamber with end offset inlet/outlet ($d = 0{\cdot}1532$ m, $l = 0{\cdot}0314$ m, $d_1 = d_2 = 0{\cdot}0486$ m, $\delta_1 = \delta_2 = 0{\cdot}0170$ m): ——, 1-D diametral; ·····, 1-D axial; - - - -, BEM.

where Z_{ch} is the characteristic impedance of the chamber given [7] by

$$Z_{ch} = \mathrm{j}\{\mathrm{H}_0^{(1)}(ka_1) - [\mathrm{H}_1^{(1)}(ka)/\mathrm{H}_1^{(2)}(ka)]\mathrm{H}_0^{(2)}(ka_1)\}/\{\mathrm{H}_1^{(1)}(ka_1) - [\mathrm{H}_1^{(1)}(ka)/\mathrm{H}_1^{(2)}(ka)]\mathrm{H}_1^{(2)}(ka_1)\}, \tag{19}$$

$H_m^{(1)}$ and $H_m^{(2)}$ being the mth order Hankel function of the first and the second kind, and a, a_1, and a_2 the radii of chamber, inlet and outlet, respectively. Figure 6 for $l/d = 0{\cdot}2050$ and Figure 7 for $l/d = 0{\cdot}1025$ compare the transmission loss of the concentric expansion chambers based on the 1-D radial, diametral, and axial models and the BEM. Both the 1-D radial and diametral solutions show reasonable agreement with the BEM predictions at low frequencies while deviating at higher frequencies. The 1-D axial predictions for these configurations lack resemblance to the other approaches, and should not be used even for estimates. The shorter chamber of Figure 7 shows that the 1-D radial prediction is closer to BEM results than the 1-D diametral model. Thus caution should be exercised in applying the 1-D diametral model to concentric configurations. The difference observed

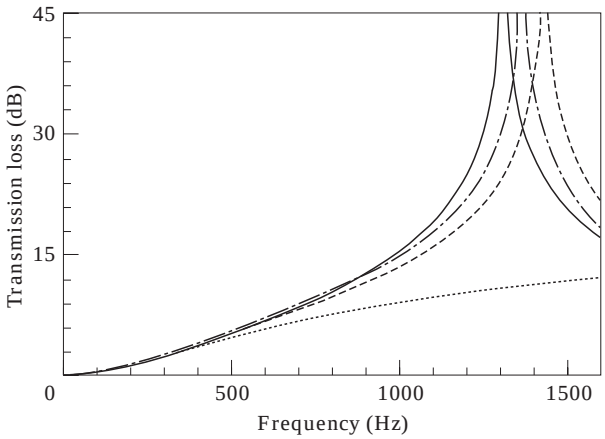

Figure 6. Transmission loss of a short concentric chamber ($d = 0{\cdot}1532$ m, $l = 0{\cdot}0314$ m, $d_1 = d_2 = 0{\cdot}0486$ m, $\delta_1 = \delta_2 = 0$): ——, 1-D radial; – · – · –, 1-D diametral; ·····, 1-D axial; - - - -, BEM.

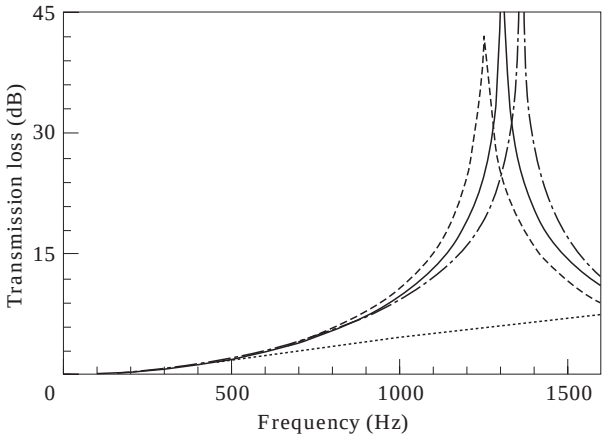

Figure 7. Transmission loss of a short concentric chamber ($d = 0{\cdot}1532$ m, $l = 0{\cdot}0157$ m, $d_1 = d_2 = 0{\cdot}0486$ m, $\delta_1 = \delta_2 = 0$): ——, 1-D radial; – · – · –, 1-D diametral; ·····, 1-D axial; - - - -, BEM.

in the resonance frequency between the 1-D radial and the BEM predictions is due to the fact that the higher order mode effects are excluded in the former. The resonance frequency based on the BEM solution moves towards lower frequencies with decreasing chamber length, while the 1-D radial ($f_{resonance} = 1305$ Hz) and diametral ($f_{resonance} = 1359$ Hz) solutions are independent of the chamber length. Similar shift to lower frequencies with decreasing l/d is also observed experimentally, as depicted in Figure 20 of reference [8]. When the two aligned inlet and outlet ducts of concentric configuration are simultaneously offset towards the perimeter of the chamber as illustrated in Figure 8(a), the 1-D diametral approach again yields reasonable predictions, as shown in Figure 8(b).

Figures 9 and 10 compare the transmission loss results of the chambers with end offset inlet/outlet, side extended inlet/outlet, and simple side inlet/outlet, from the 1-D diametral model and the BEM, respectively. The 1-D diametral results agree well with the BEM predictions at low frequencies, while deviating some at higher frequencies. For the entire frequency range the relative trends for the three configurations are consistent between the

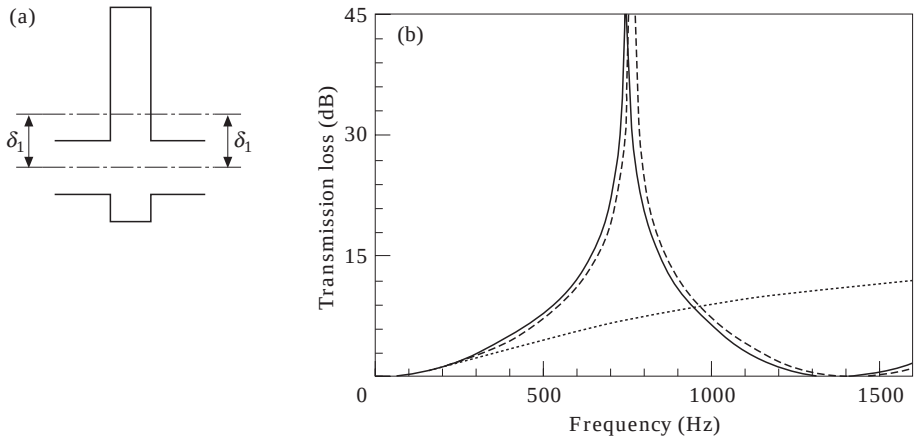

Figure 8. Transmission loss of a short chamber with end aligned inlet/outlet. (a) Layout, (b) transmission loss ($d = 0{\cdot}1532$ m, $l = 0{\cdot}0314$ m, $d_1 = d_2 = 0{\cdot}0486$ m, $\delta_1 = \delta_2 = 0{\cdot}0510$ m); ——, 1-D diametral; ·····, 1-D axial; - - - -, BEM.

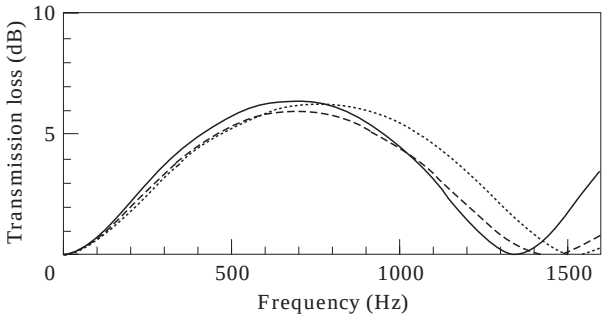

Figure 9. Transmission loss of short chambers from 1-D diametral model ($d = 0{\cdot}1532$ m, $l = 0{\cdot}0486$ m, $d_1 = d_2 = 0{\cdot}0486$ m): ——, end offset inlet/outlet ($\delta_1 = \delta_2 = 0{\cdot}0510$ m); ·····, side extended inlet/outlet ($\delta_1 = \delta_2 = 0{\cdot}0510$ m); - - - -. side inlet/outlet (no extensions).

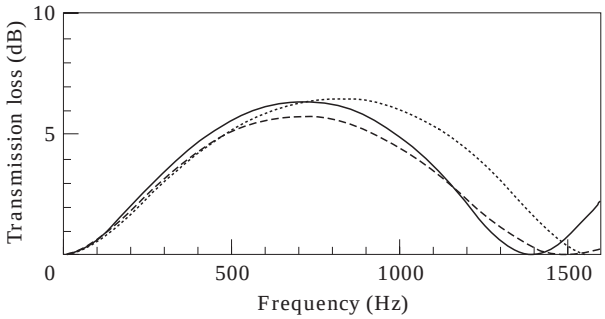

Figure 10. Transmission loss of short chambers from BEM ($d = 0{\cdot}1532$ m, $l = 0{\cdot}0486$ m, $d_1 = d_2 = 0{\cdot}0486$ m): ——, end offset inlet/outlet ($\delta_1 = \delta_2 = 0{\cdot}0510$ m); ·····, side extended inlet/outlet ($\delta_1 = \delta_2 = 0{\cdot}0510$ m); - - - -, side inlet/outlet (no extensions).

1-D model and the BEM. The side extended inlet/outlet behaves similar to the end offset inlet/outlet, except the former exhibits a wider dome due to the smaller effective length for the sound propagation in the chamber. The simple side inlet/outlet configuration reveals a smaller acoustic attenuation due to the absence of resonant end cavities.

Finally, to investigate the effect of the expansion volume, the 1-D results of transmission loss for the circular and rectangular chambers with simple side inlet/outlet

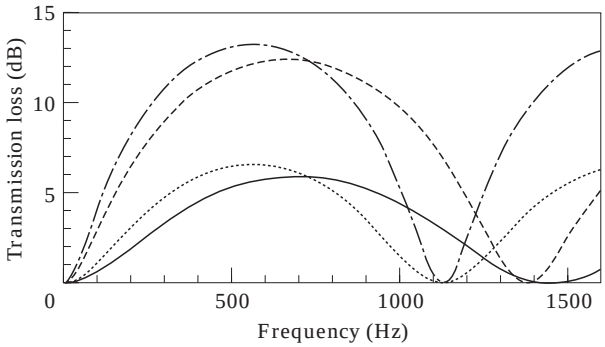

Figure 11. Transmission loss of short chambers with side inlet/outlet (no extensions) ($d = 0{\cdot}1532$ m, $l = 0{\cdot}0486$ m): ——, circular chamber ($d_1 = d_2 = 0{\cdot}0486$ m); ·····, rectangular chamber ($d_1 = d_2 = 0{\cdot}0486$ m); - - - -, circular chamber ($d_1 = d_2 = 0{\cdot}0324$ m); – · – · –, rectangular chamber ($d_1 = d_2 = 0{\cdot}0324$ m).

(no extensions) are compared in Figure 11. The rectangular configuration has the same inlet and outlet diameters and depth as the circular chamber, while the height is equal to the diameter of the circular chamber. As expected, the somewhat larger expansion volume results in a larger attenuation. The circular chamber exhibits a wider dome than the corresponding rectangular chamber due to the smaller effective length for the sound propagation in the chamber. The effect of expansion ratio is illustrated by retaining the same chambers, and reducing the inlet and outlet diameters. The transmission loss increases, as expected, while the relative trends for two configurations remain the same. With increasing frequency, multidimensional waves begin to dominate for all short chambers, terminating the applicability of the 1-D diametral model. Thus in applying this simplistic approach, the upper limit of frequency for a given configuration needs to be examined.

REFERENCES

1. D. D. Davis, G. M. Stokes, D. Moore and G. L. Stevens 1954 *NACA TN* 1192. Theoretical and experimental investigations of mufflers with comments on engine exhaust muffler design.
2. A. Selamet, Z. L. Ji and P. M. Radavich 1998 **213,** 601–617. *Journal of Sound and Vibration*. Acoustic attenuation performance of circular expansion chambers with offset inlet/outlet: I analytical approach.
3. A. Selamet and Z. L. Ji 1998 **213,** 619–641. *Journal of Sound and Vibration*. Acoustic attenuation performance of circular expansion chambers with offset inlet/outlet: II. comparison with computational and experimental studies.
4. Z. L. Ji and J. Z. Sha 1995 *Journal of the Acoustical Society of America* **98**, 2848–2850. Four-pole parameters of a duct with low Mach number flow.
5. V. H. Gupta 1996 *Journal of the Acoustical Society of America* **99**, 1862–1867. A proof of the convergence of the segmentation approach used in analysis of one-dimensional linear system.
6. M. J. Munjal 1987 *Acoustics of Ducts and Mufflers*. New York: Wiley-Interscience.
7. N. S. Dickey and A. Selamet 1996 *Journal of Sound and Vibration* **195**, 512–517. Helmholtz resonators: one-dimensional limit for small cavity length-to-diameter ratios.
8. A. Selamet and P. M. Radavich 1997 *Journal of Sound and Vibration* **201**, 407–426. The effect of length on the acoustic attenuation performance of concentric expansion chambers: an analytical, computational, and experimental investigation.